Modulating acrylic acid content of nanogels for drug delivery & biocompatibility studies

Anuvansh Sharma [a], Karthik Raghunathan [b], Helene Solhaug [c], Jibin Antony [b], Jørgen Stenvik [d,e], Asbjørn Magne Nilsen [e], Mari-Ann Einarsrud [a], Sulalit Bandyopadhyay [b,*]

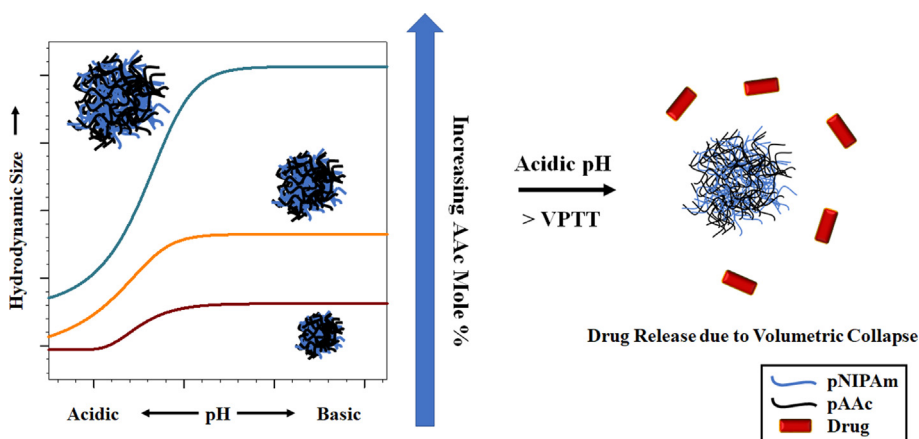[a] Department of Materials Science and Engineering, NTNU Norwegian University of Science and Technology, Norway
[b] Department of Chemical Engineering, NTNU Norwegian University of Science and Technology, Norway
[c] Department of Clinical and Molecular Medicine, Faculty of Medicine and Health Sciences, NTNU Norwegian University of Science and Technology, Trondheim, Norway
[d] Centre of Molecular Inflammation Research, NTNU Norwegian University of Science and Technology, Trondheim, Norway
[e] Department of Clinical and Molecular Medicine, NTNU Norwegian University of Science and Technology, Trondheim, Norway

GRAPHICAL ABSTRACT

ARTICLE INFO

ABSTRACT

Dual stimuli-responsive nanogels (NGs) have gained popularity in the field of bio medicine due to their versatile nature of applicability. Poly(N-isopropylacrylamide)-co-poly(acrylic acid) (pNIPAm-pAAc)-based NGs provide such dual stimuli-response with pNIPAm and pAAc providing thermal and pH-based responses, respectively. Studying the growth of these NGs, as well as, understanding the effect of the incorporation of pAAc in the NG matrix, is important in determining the physico-chemical properties of the NG. Studies have been conducted investigating the effect of increasing pAAc content in the NGs, however, these are not detailed in understanding its effects on the physico-chemical properties of the pNIPAm-pAAc-based NGs. Also, the biocompatibility of the NGs have not been previously reported using human whole blood model. Herein, we report the effect of different reaction parameters, such as surfactant amount and reaction atmosphere, on the growth of pNIPAm-pAAc-based NGs. It is shown that the size of the NGs can be precisely controlled from ~130 nm to ~400 nm, by varying the amount of surfactant and the reaction atmosphere. The effect of increasing incorporation of pAAc in the NG matrix on its physico-chemical properties has been investigated. The potential of these NGs as drug delivery vehicles is investigated by conducting loading and release studies of a model protein drug, cytochrome

* Corresponding author.
 E-mail address: sulalit.bandyopadhyay@ntnu.no (S. Bandyopadhyay).

Abbreviations

AAc	Acrylic acid		NMR	Nuclear magnetic resonance
BIS	N-N′-methylene-bisacrylamide		PFA	Paraformaldehyde
CR3	Complement Receptor 3		PSD	Particle size distribution
CS	Continuous-Stirring		PBS	Phosphate buffered saline
Cyt *C*	Cytochrome *C*		pAAc	Poly(acrylic acid)
DLS	Dynamic light scattering		PDI	Polydispersity index
E.E.	Encapsulation efficiencies		pNIPAm	Poly(N-isopropylacrylamide)
FI	Flashing-Impeller		PI	Propidium iodide
FS	Flashing-Stirring		SDS	Sodium dodecyl sulpahate
KPS	Potassium persulphate		TCC	Terminal complement complex
LPS	Lipopolysaccharide		TMB	Tetramethylbenzidine
L.E.	Loading efficiency		TEM	Transmission electron microscopy
NGs	Nanogels		VCE	Volumetric collapse efficiency
NIPAm	N-isopropylacrylamide		VPTT	Volume phase transition temperature

C (Cyt *C*) from the NGs at temperature above the volume phase transition temperature (VPTT) and acidic pH. An *ex vivo* human whole blood model was used to investigate biocompatibility of the NGs by quantifying inflammatory responses during NG exposure. The NGs did not induce any significant production of chemokine IL-8 or pro-inflammatory cytokines (IL-1β, IL-6, TNF-α), and the cell viability in human whole blood was maintained during 4 h exposure. The NGs did neither activate the complement system, as determined by low Terminal Complement Complex (TCC) activation and Complement Receptor 3 (CR3) activation assays, thereby overall suggesting that the NGs could be potential candidates for biomedical applications.

---

1. Introduction

Stimuli-responsive nanogels (NGs) have been shown to have great potential in biomedical applications, such as drug delivery [1] and tissue engineering [2]. Owing to the complexity of the physiological microenvironments, NGs responding to a single stimuli might not be suitable to achieve the desired goals, therefore, materials that are responsive to more than one physical or chemical stimuli are highly desired for biomedical applications [3]. Poly (N-isopropylacrylamide)-co-poly(acrylic acid) (pNIPAm-pAAc)-based NGs provide exactly such dual stimuli response with temperature and pH [4,5]. pNIPAm-based NG undergoes entropically driven reversible coil-to-globule phase transition above the volume phase transition temperature (VPTT), owing to the hydrophilic amide and hydrophobic propyl groups, that lies around 36 °C for these systems, thereby making them most widely studied thermosensitive polymers for biomedical applications of targeted drug delivery [6,7]. The VPTT of pNIPAm-based NGs can be altered by copolymerizing NIPAm with other hydrophobic or hydrophilic monomers [8,9] and acrylic acid (AAc) is one such hydrophilic monomer that also imparts pH response to the polymer, as previously shown by our group [10,4].

PNIPAm-pAAc-based NGs are usually synthesized using precipitation polymerization at temperatures above the VPTT of the formed NG [11,12,4]. A surfactant, such as sodium dodecyl sulphate (SDS), is generally added to avoid NG agglomeration and control the population size [13–15]. These reactions are extremely sensitive to synthesis parameters, including, reactant concentrations, surfactant concentration, amount of initiator and reaction temperature. Studies conducted by Lyon et al. and our group, have shown the effect of these parameters on the size of NGs [10,16]. The presence of oxygen has been shown to hamper radical polymerization reactions by reacting with either the initiator, primary or the growing polymer radical units forming peroxides that hinder further chain growth [17–19]. However, the effect of oxygen atmo-

sphere has not yet been investigated for the synthesis of pNIPAm-pAAc based NGs. Furthermore, polymerization occurs rather fast upon addition of the initiator, thereby shortening the nucleation window. Thereafter, chain growth takes place, where the polymer and co-polymer are incorporated within the NG matrix. The reaction is complex and few studies have been conducted to understand the growth of pNIPAm-based gels [15,20]. In addition, to understand the stimuli response from temperature and pH, it is important to study the extent of incorporation of pNIPAm and pAAc in the NG matrix. Studies have shown the effect of increasing amounts of AAc on the physico-chemical properties [21–23], as well as, the loading efficiencies of the NGs with cytochrome *C* (Cyt *C*) [10,24] and l-dopa [25,26]. Our group, among others, have shown loading and release of drugs from pNIPAm-pAAc based gels at different conditions of temperature and pH [10,25,24,27]. However, most of these studies are not associated with NGs, but, microgels and they do not highlight in detail, the effect of pAAc on the physico-chemical properties, such as swelling/collapse and VPTT of the NGs, as well as, release of drug from these NGs. Although, NGs and microgels share similar structures, NGs pose an advantage owing to their smaller size and responsiveness to deliver payloads to target areas, together with high drug encapsulation, large surface area, and stable interior network structure [28–30].

As the effect of drug carriers increases with circulation time in the blood stream, investigating inflammatory responses in a blood model can be important to gain information on the biocompatibility of the system [31]. Inflammatory responses in blood during exposure to potential drug carriers and NPs can be determined by quantifying pro-inflammatory cytokine production, the formation of the complement activation product soluble Terminal Complement Complex (TCC) and activation of the Complement Receptor 3 (CR3) [32,33]. Previous studies suggests that NGs with AAc as comonomers, have low cytotoxicity and do not induce production of pro-inflammatory cytokines [34,35]. However, the models used are often solely based on *in vitro* cell mono-cultures, i.e.

monocytes lacking the complex interaction between different cell types and plasma cascades involved in an *in vivo* response scenario, as can be modelled using human whole blood [36]. Release of cytokines, such as chemokine IL-8 and pro-inflammatory cytokines IL-1β, IL-6 and TNF-α, have been suggested as potent biomarkers for predicting the immunotoxic potential of NPs, due to high levels of induction being closely related to change in cellular mechanisms and toxicity [37].

In this study, we performed time-based growth experiments to study the formation of pNIPAm-pAAc-based NGs by varying selected reaction parameters, primarily surfactant amounts and reaction atmosphere, to investigate their effects on the physico-chemical properties of the NGs. In addition, the effect of the extent of AAc incorporation in the NG matrix on the physico-chemical properties of the NG was studied. The potential of these NGs as drug delivery vehicles was evaluated by performing loading and release of Cyt *C*, a model protein drug, at different conditions of temperature and pH, and for the first time, using NGs with varying pAAc incorporation in the matrix. Furthermore, biocompatibility studies were conducted on the pNIPAm-pAAc based NGs using a human whole blood model, which is an *ex vivo* model allowing to study the complexity of complement activation by closely mimicking the *in vivo* conditions [36].

2. Experimental section

N-isopropylacrylamide (NIPAm, 97%), N-N′-methylene-bisacrylamide (BIS, 99%), acrylic acid (AAc, 99%), sodium dodecyl sulphate (SDS, 99%), potassium persulphate (KPS, >99%), phosphate buffered saline (PBS, suited for cell culture, endotoxin tested, and supplemented with Ca^{2+}/Mg^{2+}, Zymosan (A crude cell wall extract from the yeast *Saccharomyces cerevisiae*) and propidium iodide (PI) solution suitable for hematology ($\geqslant 94\%$) were purchased from Sigma–Aldrich® (Schnelldorf, Germany). Ethylenediaminetetraacetic acid (EDTA, ultrapure grade, 0.5 M) was purchased from Invitrogen (Waltham, MA, USA). Ultrapure lipopolysaccharide (LPS) from *Escherichia coli* serotype O111:B4 was purchased from InvivoGen (San Diego, CA, USA). Sterile Refludan for injection or infusion containing the thrombin inhibitor Lepirudin (50 mg/mL) was purchased from Pharmion (Windsor, UK). Lysis buffer and anti-CD11b labelled with phycoerythrin (PE) for flow cytometry were purchased from BD Biosciences (Franklin Lakes, NJ, USA). Paraformaldehyde aqueous solution for cell fixation (PFA, 16%, methanol free and microfiltered) was purchased from VWR (Radnor, PA, USA). All the chemicals (except NIPAm) were used as received without any further purification or modification. Solutions for whole blood experiments were prepared in PBS with Ca^{2+}/Mg^{2+}, which are essential for normal complement activation. All other solutions were prepared using distilled de-ionized water (MQ-water), having a resistivity ∼18.2 MΩ.cm at 25 °C, taken from Simplicity® Millipore (Darmstadt, Germany) water purification system.

2.1. Recrystallization of NIPAm

To remove impurities that could inhibit the polymerization reaction, NIPAm was recrystallized using a previously reported protocol by our group [10]. In a typical process, 5 g of NIPAm was dissolved in 50 mL of n-hexane in a one-necked round bottom flask maintained at 110 °C using an oil bath. The reaction was allowed to proceed for 2 h following which, the reactor was placed over an ice bath for 30 min, to allow recrystallization of NIPAm. The solution was then filtered using a $\phi - 90$ mm filter paper and kept for overnight drying. After drying, the recrystallized NIPAm was stored at −20 °C to prevent absorption of moisture.

2.2. Synthesis of nanogels

The NGs were synthesized using precipitation polymerization as previously reported by our group [10]. The monomers NIPAm and AAc were used to synthesize the NGs using BIS as cross-linker; SDS was used as surfactant and the reaction proceed by adding KPS, as an initiator. In a typical reaction, NIPAm (181 mg) and BIS (14.5 mg) were added to a round bottom flask maintained at 70 °C. 10 mL of SDS, with different molarities (4.2, 3.5, 2.8 and 2.1 mM), were added to the flask and the reaction mixture was stirred for 1 h to ensure the collapse of all NIPAm monomeric units. After 1 h, AAc (124 μL of 1.46 M) and KPS (400 μL of 103 mM) were added in quick succession and the reaction was allowed to continue for 3 h.

To investigate the effect of reaction environment (atmosphere), three different modes of synthesis were applied, namely, a) Continuous-Stirring (CS) – maintaining continuous flow of N_2 with stirring using a magnetic bar stirrer, b) Flashing-Stirring (FS) – N_2 purging during addition of the initiator with stirring using a magnetic bar stirrer, and c) Flashing-Impeller (FI) – N_2 purging during addition of the initiator with stirring using an impeller. Fig. 1 represents the schematic of the three synthesis techniques used based on N_2 usage and the method of stirring. All the synthesised NGs were dialysed overnight using a 14 kDa molecular weight cut-off (MWCO) dialysis membrane, to remove any unreacted monomers and residual reactants. The dialysed NGs were freezedried to remove the solvent and stored at 4 °C for further analysis.

Furthermore, to investigate the pH stimuli response of the NGs with increased incorporation of pAAc units in the NG matrix, NGs were synthesised using CS method. The mole ratios of the monomer (NIPAm), co-monomer (AAc) and crosslinker (BIS) were varied for the different NG samples, as shown in Table 1.

2.3. VPTT Calculation

VPTT of the NGs was calculated by plotting the swelling/collapse of the NGs over a temperature range for both, the heating and cooling cycles. The sizes of these NGs were measured using dynamic light scattering (DLS), between 25 and 55 °C with an interval of 5 °C. Using the NG sizes at different temperatures, relative swelling of the NGs (α_T) was calculated as described in Eq. 1.

$$\alpha_T = \left\{ \frac{D}{D_0} \right\}^3 \tag{1}$$

where, D is the NG's hydrodynamic diameter at a given temperature and D_0, is the diameter at 25 °C. α_T was plotted against temperature for heating and cooling cycles and a sigmoidal 5 parameter equation (Eq. 2) was fit, using SigmaPlot® version 14.0, to the obtained curves to find the VPTT described in our previous work [38].

$$y = y_0 + \frac{a}{\left[1 + e^{-\left(\frac{x - x_0}{b}\right)} \right]^c} \tag{2}$$

where, a, b, c, x_0 and y_0 are the 5 constant parameters obtained from SigmaPlot®. An in-house developed MATLAB® code was used to calculate the system's VPTT by equating the areas under the heating and cooling curves, measured by Simpson's $1/3^{rd}$ rule [38].

2.4. VCE_{temp} and VCE_{pH} Calculations

At temperatures above VPTT and acidic pH, NGs undergo volume based collapse. Drug release studies involving polymeric NPs were conducted at different temperature conditions that are usually above the transition temperatures of the material (∼37 – 45 °C) [39–42]. Furthermore, it is seen that the biological microenvironment surrounding cancer cells tends to be acidic compared to
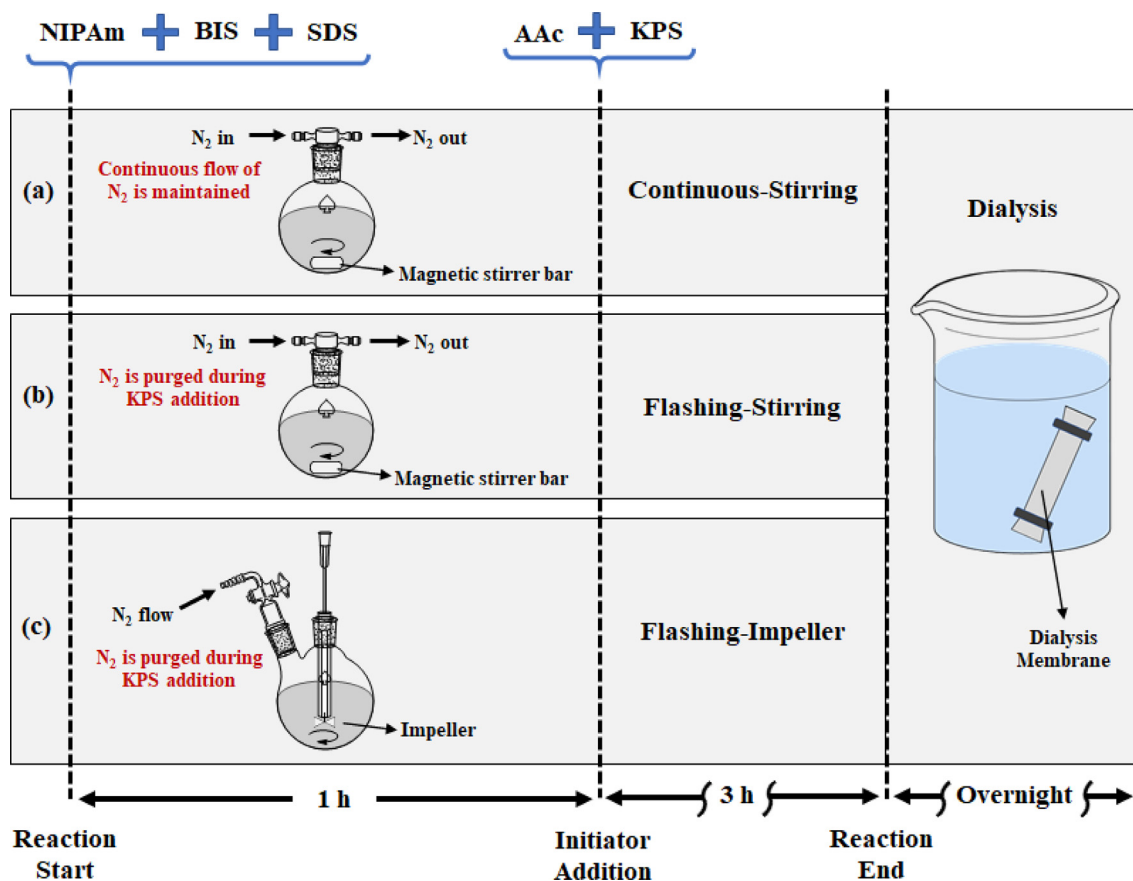
Fig. 1. Schematic representation of the synthesis of NGs via a) Continuous-Stirring, b) Flashing-Stirring, and c) Flashing-Impeller techniques, showing the different nitrogen and stirring modes used in the three synthesis methods.

Table 1
Varying monomer, co-monomer and crosslinker concentrations to study the effect of incorporation of pAAc (in the NG matrix) on the pH response of the NG.

Sample	Mole Ratio NIPAm:AAc:BIS	NIPAm (mg)	AAc (µL)	BIS (mg)
AAc_10	85:10:05	181	129	14.5
AAc_12.5	82.5:12.5:05	181	166	14.9
AAc_15	80:15:05	181	205	15.4
AAc_17.5	78.5:17.5:05	181	247	15.9
AAc_20	75:20:05	181	292	16.4
AAc_22.5	72.5:22.5:05	181	340	17.0
AAc_25	70:25:05	181	391	17.6
AAc_27.5	68.5:27.5:05	181	446	18.3
AAc_30	65:30:05	181	506	19.0

that of normal blood (pH = 7.4), providing optimum conditions for cancer growth [43–45]. Hence, the volumetric collapse efficiencies (VCE) of the NGs, with respect to temperature (25 and 45 °C – maximum collapse of NGs) and pH (3.5 and 7.4), were calculated based on Eqs. 3 and 4 respectively.

$$VCE_{temp} = \frac{D_{25}^3 - D_{45}^3}{D_{25}^3} \times 100\% \qquad (3)$$

$$VCE_{pH} = \frac{D_{7.4}^3 - D_{3.5}^3}{D_{7.4}^3} \times 100\% \qquad (4)$$

where, VCE_{temp} is the volumetric collapse efficiency based on the temperature response of the NG (measured at normal pH) and VCE_{pH} is the volumetirc collapse efficiency based on the pH

response of the NG (measured at 25 °C). D_{25} and D_{45}, are NG's hydrodynamic diameters at 25 and 45 °C, respectively. $D_{3.5}$ and $D_{7.4}$ are the hydrodynamic diameters at pH = 3.5 and 7.4, respectively.

2.5. Drug loading and release

A model protein drug, Cyt C, was used to perform loading and release studies from NGs synthesized via CS and FS methods. Breathing in technique was used to load Cyt C, wherein, a freeze-dried NG sample was suspended in the drug solution to allow absorption of Cyt C in the NG matrix as the hydrophilic NG swells in solution. In a typical study, 1.7 mg of freeze-dried NG sample was taken in a glass vial and 2 mL of 0.5 mg/mL Cyt C solution was added. The mixture was kept for shaking at 300 rpm for 2 h following which the sample was dialysed for 24 h in MQ water using a 14 kDa molecular weight cut-off (MWCO) membrane tubing to remove unbound drug from the system. The sample was then re-suspended in 5 mL water for release measurements. The absorbance value of Cyt C was measured using UV–vis spectrophotometer at 409 nm and loading efficiency (L.E.) of the NGs was calculated using Eq. 5.

$$L.E.(\%) = \frac{Abs_{dia}}{Abs_{CytC}} \times 100\% \qquad (5)$$

where, Abs_{dia} and Abs_{CytC} are the absorbance values of Cyt C of the dialysed sample and that of the drug solution time = 0 and at a particular time 'i', respectively.

Cyt C release studies was performed at different temperature (above VPTT of NGs) and pH (acidic) conditions over a period of

time. Absorbance value of Cyt *C* at 409 nm was measured and the drug release % was calculated using Eq. 6.

$$Release(\%) = \frac{Abs_{t0} - Abs_{ti}}{Abs_{t0}} \times 100\% \qquad (6)$$

where, Abs_{t0} and Abs_{ti} are the absorbance values of Cyt *C* at time = 0 and at a particular time 'i', respectively.

2.6. Whole blood model

Human whole blood, from voluntary healthy donors, was collected in low-activating polypropylene vials (Nunc 4.5 mL) containing thrombin inhibitor/anti-coagulant lepirudin (50 μg/mL). Immediately after collection, 500 μL blood and controls were incubated with 200 μL NGs in 1.8 mL Nunc propylene vials. Phosphate buffered saline (PBS) was used as the negative control while Zymosan and Lipopolysaccharide (LPS) served as positive controls with final concentrations of 10 μg and 100 ng/mL, respectively. The NGs were added with final concentrations of 1, 10 and 100 μg/mL. The tubes were then incubated at 37 °C in a Rock'n Roller (Labinco B.V., The Netherlands) providing continuous, slow rotation around the axis of the tubes at a fixed angle. Samples were extracted from the tubes after a given incubation time according to the response parameters that were examined; TCC: 30 min, cytokine production and cell viability: 240 min. For TCC and cytokine analysis, EDTA (final concentration = 10 mM) was added to stop further potential complement activation. Plasma was then separated by centrifuging the whole blood samples at 1800 times *g* for 15 min. Plasma was stored at −20 °C until analysis.

2.6.1. TCC activation

TCC formation analysis were performed using a TCC ELISA kit (Human Terminal Complement Complex HK328, Hycult Biotech, Netherlands), according to the instructions from the manufacturer. In brief, plasma samples and controls were added to the antibody-covered 96-well plate and incubated for 1 h at room temperature, followed by washing with wash buffer. Biotinylated tracer was added followed by another 1 h incubation step. After washing with the wash buffer, streptavidin-peroxidase conjugate was added and the plate was further incubated for 1 h. The wells were then washed again before tetramethylbenzidine (TMB) was added and incubated for 30 min. Kit stop solution was added before the plate was read at 450 nm using a UV–vis spectrophotometer (Unico, Dayton, OH, USA).

2.6.2. Cytokine production

The concentrations of the pro-inflammatory cytokines IL-1β, IL-6, IL-8 and TNF-α were determined using Bio-Plex Pro Human Cytokine Screening Panel assay kit (BioRad, Hercules, CA, USA). The assay was performed per the manufacturers instructions. In brief, assay bead solution was diluted and added to a Bio-Plex Pro 96-well assay plate. Plasma samples and recombinant reference cytokines (standards) were diluted in Bio-Plex sample dilution buffer and added to the beads. The assay plate was then incubated on a shaker for 30 min at 850 ± 50 rpm before it was washed three times. Detection antibody was added, followed by another 30 min of incubation on the shaker. After washing, streptavidin-peroksidase was added to the plate followed by 10 min incubation on the shaker. After another washing step, Bio-Plex assay buffer was added and the plate was shaken for 30 s. The beads were analysed using Bio-Plex 200 with Bio-Plex Manager Software.

2.6.3. Cell viability

25 μL whole blood samples were transferred to separate flow vials after 4 h incubation. Non-treated fresh blood was used as neg-

ative control of cell death, while as positive control blood cells were killed by heating the blood for 2 min at 70 °C followed by 3 min on ice. 2.5 μL propidium iodide (PI) was added shortly before flow cytometry analysis with BD FACSCanto II (BD BioSciences, Franklin Lakes, NJ, USA). NG induced cytotoxicity in monocytes and granulocytes was quantified by, first gating living and dead cell populations in the negative and positive controls according to their forward- and side scatter, and then applying the same gating for the NG treated samples. This data analysis was done using FlowJo software (BD BioSciences).

2.7. Characterization techniques

2.7.1. Dynamic Light Scattering (DLS) and zeta potential measurements

The size distribution and zeta potential of the NGs were measured using a Malvern Zetasizer Nano-ZS instrument (Malvern Instruments Ltd., Worcestershire, UK). All the NG solutions were made using MilliQ water and results were averaged over triplicate measurements.

2.7.2. Transmission Electron Microscopy (TEM)

TEM characterization was performed using JEOL JEM-1011 with tungsten filament, with accelerated voltage of 80 kV. Images were captured with MORADA CCD camera (3392 x 2248 x 16bit). NGs were stained using uranyl acetate. The NGs were diluted to 0.2 mg/mL suspension and equilibrated at room temperature for 5 h before sonication for 1 min. Uranyl acetate solution (1 mL, 4%) was added to 1 mL NG suspension and equibrilated for 15 min. Drops were placed on sterile copper grids with formvar and allowed to rest for 5 min before carefully dried on the edges using filter paper. The grid was air dried for 24 h before characterization.

2.7.3. Nuclear Magnetic Resonance (NMR)

^{1}H NMR spectra were recorded in a Bruker Advance Neo 600 MHz instrument. All samples were prepared in heavy water (D_2O) keeping the reagent concentrations the same as that in the NG synthesis. 0.8 mL suspension was taken from each sample and the spectra were recorded with 128 scans at 25 °C. The reference peak was locked at 4.80 for D_2O. Chemical shifts (δ) were reported in ppm.

3. Results and discussion

3.1. NG synthesis methods and growth kinetics

The hydrodynamic sizes presented in Fig. 2a, show the temperature dependent size change of the NGs at different SDS concentrations. NGs synthesized by continuous-stirring method (NGs_CS) show an increasing hydrodynamic diameter from 208 ± 2 nm to 373± 4 nm when the SDS amount was decreased from 4.2 to 2.1 mM, respectively. Similar trend can also be observed for the NGs synthesized by flashing-stirring (NGs_FS) and flashing-impeller (NGs_FI) methods. In the course of NG formation, SDS provides colloidal stability to the precursor particles during nucleation by electrostatic stabilization [46]. In addition to providing charge stabilization, a higher concentration of SDS results in denser packing around the incipient nucleation (oligomer) centers, thereby limiting the growth of NGs. These data confirm results obtained in previous studies conducted by our group, where SDS concentration was one of the central factors determining the size of the NGs [10]. Furthermore, all the NGs show temperature stimulated volume based transition when exposed to temperatures above their
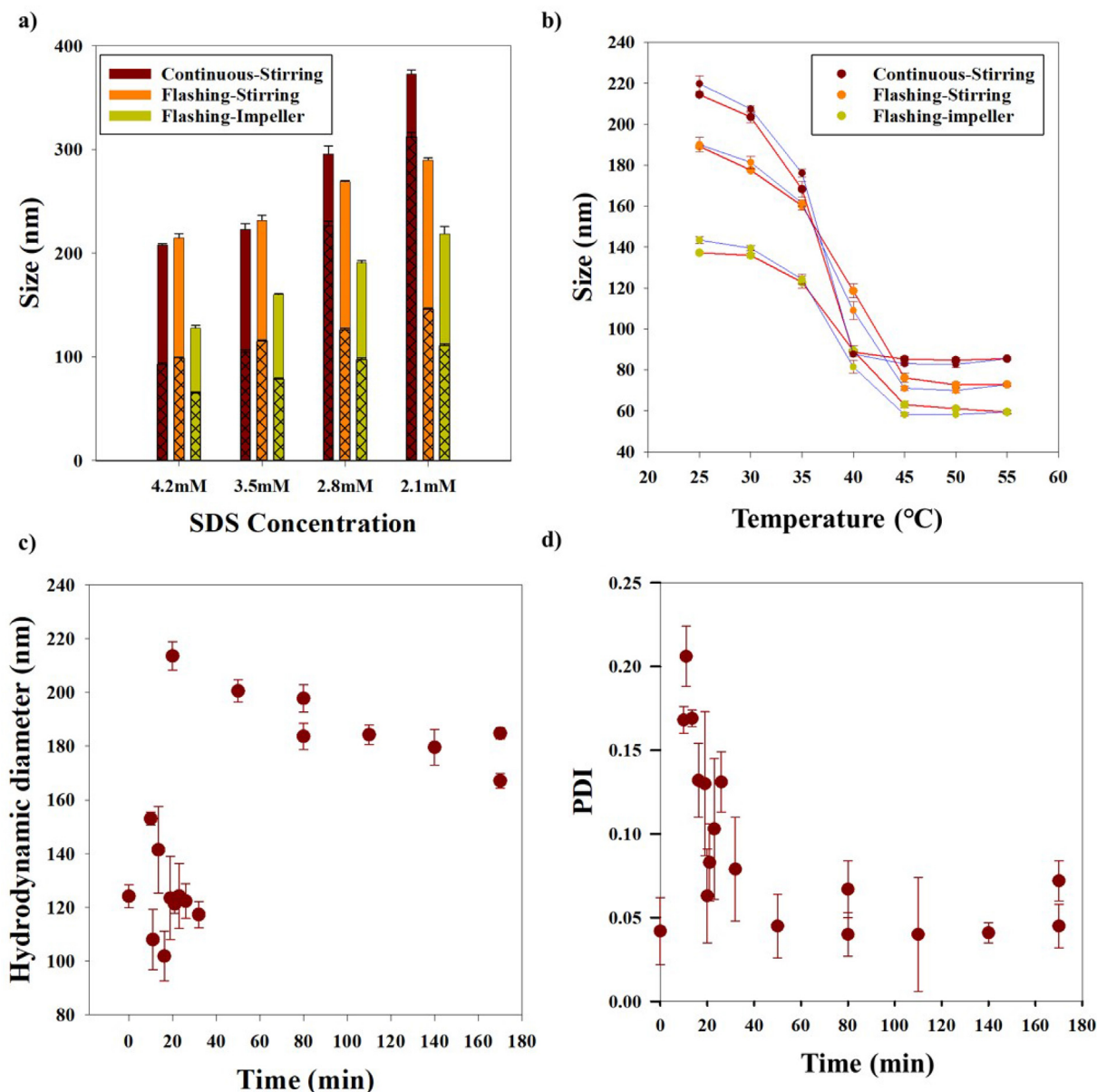
Fig. 2. Variation in the sizes of NGs, synthesized via continuous-stirring, flashing-stirring and flashing-impeller methods, as a function of a) surfactant (SDS) concentration (black crosshatches represent the sizes of NGs at 45 °C) and b) temperature (at 4.2 mM SDS). Variation of c) size and d) PDI, as a function of reaction duration for NGs synthesised using continuous-stirring method, showing the progress of the reaction, with the size increasing and PDI decreasing as the reaction proceeds. The error bars represent the standard deviation calculated from the triplicate measurement of the particular sample.

VPTT. The reduction in NG sizes at 45 °C have been shown by an overlay (black grids) on the corresponding NGs bar curves in Fig. 2a. An entropy driven release of bound water molecules takes place at elevated temperatures due to breaking of hydrogen bonds. Thus, polymer–polymer interactions become stronger than polymer–solvent interactions leading to phase separation and collapse of the NGs.

The heating and cooling phase transition curves, shown in Fig. 2b, are used to determine the VPTTs of the respective NG systems, presented in Table 2. All the NGs showed collapse above VPTT, leading to visible colour change from transparent to pale whitish as the solution turned turbid. The curves in Fig. 2b have a sigmoidal shape, however the collapse for NGs_CS was more abrupt than for the other two systems. Low PDI, measured using Eq. 7 [47] for NG_CS depicts more monodisperse particles than NGs_FS and NGs_FI (Table 2).

Table 2
VPTT and PDI of NGs synthesized by different methods using 4.2 mM SDS.

Method Used	VPTT (°C)	PDI
Continuous-stirring	36.3 ± 0.1	0.2 ± 0.0
Flashing-stirring	37.8 ± 0.1	0.7 ± 0.1
Flashing-impeller	37.7 ± 0.1	0.6 ± 0.2

$$\sigma = \frac{\left(\overline{a^2} - \overline{a}^2 \right)^{1/2}}{\overline{a}} \tag{7}$$

where, $\overline{a^2}$ is the NG's mean size and $\overline{a}$ is the NG size.

Having a narrower particle size distribution (PSD) might lead to a more uniform and consistent collapse of the entire system as a whole. In the case of NGs_FS and NGs_FI, with a broader PSD, non-uniform collapse of all the particles at a particular tempera-

ture will occur, resulting in a gradual slope in size collapse (Fig. 2b). The three NGs have temperature-based volumetric collapse efficiencies (VCE$_{temp}$) that follow the order; NGs_CS > NGs_FS > NGs_FI (for 4.2 mM SDS), as seen in Table 3. Low VCE$_{temp}$ was also witnessed in our previous studies for NGs_CS method [10], however, low VCE$_{temp}$ was not seen in the case of NGs_FS > NGs_FI in this study. High VCE$_{temp}$ highlights the fact that the hydrophobic tails of the SDS chains interfere constructively in increasing the hydrophobicity of the NGs above VPTT, whereby causing a more efficient collapse. Low VCE$_{temp}$, in the case of NGs_CS, at low SDS concentrations reflects lower incorporation of SDS in the NGs, thereby making the system more hydrophilic with lower collapse. NGs have smaller sizes at 2.8 and 2.1 mM SDS for FS and FI methods, indicating the possibility of higher SDS present in the NG, resulting in more efficient volume collapse at lower SDS concentrations.

Fig. 2c and 2d show the variation of particle size and PDI with respect to reaction time for NGs_CS. Time 't = 0' represents the time of initiator addition and the reaction continued for 3 h after the addition. Smaller particle sizes and high PDI were observed in the initial stages of polymerization. The size and PDI values vary a lot in the initial stages of polymerization with high standard deviation which stabilize as the reaction proceeds. A rapid increase in the size of the particles was observed corresponding to the transfer to the pale whitish colour of the reaction medium. This increase in size was different for the three systems with NGs_FI having the fastest increase while NGs_CS having the slowest increase (Fig. S1). ^{1}H NMR of the different NGs showed similarity in the polymer matrix regardless of the synthesis method used, with the typical characteristic proton peaks, ascribed to pNIPAm and the overlapping peaks of pAAc, as can be seen Fig. S3 [48]. NGs from the three methods showed peaks at around 1.0 ppm and 3.8 ppm for the free –CH$_3$ and –CH$_2$– groups of pNIPAm, respectively. The peaks for the protons of pNIPAm and pAAc, that are present in the polymer backbone, were overlapping in the region 1.4–2.2 ppm. Thus, the differences in the NG structures from ^{1}H NMR could not be predicted.

The reaction medium in the case of NGs_CS is maintained under oxygen-free atmosphere throughout the whole reaction. For the NGs_FS and NGs_FI, nitrogen was purged for 5 min after initiator (KPS) addition, however, the reaction was further maintained under sealed atmosphere (reactor) in the former case, thereby shielding the medium from oxygen for the initial stages of the reaction involving, initiator (KPS) activation and commencement of polymerization. Whereas, in the case of NGs_FI, the seal at the

reactor neck, where the impeller rod enters the reactor, doesn't make an airtight seal, thereby having a possibility of air entering the reactor and exposing the reaction mixture to oxygen. The presence of oxygen might be responsible for reducing the efficiency of the initiator as well as cause untimely polymer chain terminations, thereby resulting in smaller polymer chains. This further result in smaller sizes of the NGs (Fig. S1), together with higher PDI for these systems, as compared to NGs_CS and NGs_FS, despite showing structure similarity from ^{1}H NMR (Fig. S3). Fig. 2d shows the variation of PDI of NG_CS as a function of reaction time. PDI follows a similar trend as NG size with high degree of deviation during the initial stages of the reaction and stabilizing as polymerization proceeds. Also, the impeller creates a greater shear as opposed to stirring with a bar magnet, that might result in more reaction nuclei being formed thereby reducing the final NG size. The reaction kinetics of NGs_CS is slowest among the three methods and the final particle size is reached after an hour of KPS addition. NGs_FI are the fastest at attaining the final particle size, whereas the kinetics of NGs_FS lies in between the other two methods. Therefore, less number of nuclei form for NGs_CS, leading to greater growth of NGs and larger particle size. Stirring by impeller could also assist in capturing oligomers more efficiently resulting in earlier onset of polymerization, as seen by the earlier colour change of the reaction mixture. It can further assist in stabilizing these nuclei by providing better access to SDS in the reaction mixture.

As NGs_CS had the highest VCE$_{temp}$ (91.9 ± 0.7) (Table 3), this system was selected to study the effect of increased incorporation of pAAc in the NG, on its physico-chemical properties.

3.2. Effect of Acrylic Acid (AAc)

To investigate the effect of increasing number of pAAc chains in the NG matrix, the mole% of AAc monomers, in the NG_CS samples, was increased from 10 to 30 with an interval of 2.5 (Table 1).

Fig. 3a and b show the variation in the hydrodynamic diameter and zeta potentials for different mole% of AAc (Table 1) with respect to temperature (25 and 45 °C) and pH (3.5 and 7.4). The NGs show collapsing trend with increasing temperature in contrast to swelling behaviour when transferring from acidic to basic medium. The collapse of the NGs above their VPTTs (between 34 and 36 °C in our case (Table S1), is primarily due to a shift in the balance of hydrophilic/ hydrophobic forces that cause coil-to-globule transition upon increase in temperature. At elevated temperatures, entropically-driven release of bound water takes place due to breakage of hydrogen bonds, and water is excluded from the molecular aggregates as polymer–polymer interactions exceed polymer–solvent interactions. The polymer chains, thus collapse, attaining a globular structure resulting in phase separation [10].

The hydrophobicity of AAc increases below pKa of ≈4.26 due to protonation of the carboxylic (–COOH) groups, leading to the formation of hydrogen bonds between the carboxylic groups. This increases the crosslinking within the NG thereby reducing the diffusion of water into the NG matrix making them denser. As AAc deprotonates at higher pH and becomes negatively charged, repulsion between the polymeric chains occurs. The maximum stretching of the polymeric chain with deprotonation depends on the percent ionization of the carboxylic groups. Therefore, a higher amount of AAc in the NG matrix is expected to promote swelling of the structure.

The variations in VCE of the NGs with temperature and pH are shown in Fig. 3c. VCE$_{temp}$ and VCE$_{pH}$, show a decreasing and an increasing trend with the varying amounts of initial AAc content, respectively. The increase in VCE$_{pH}$ can be attributed to the increasing number of AAc units being incorporated in the NG matrix, thereby occupying more sites within the network. Hence,

Table 3
VCE$_{temp}$ of NGs_CS, NGs_FS and NGs_FI, synthesized using continuous and flashing methods at different SDS concentrations.

SDS mMole	Continuous-stirring %	Flashing-stirring %	Flashing-impeller %
4.2	92 ± 0	90 ± 1	87 ± 1
3.5	90 ± 1	88 ± 1	88 ± 0
2.8	55 ± 8	90 ± 1	87 ± 1
2.1	41 ± 5	87 ± 1	87 ± 1

Table 4
Extent of collapse of NGs_CS with temperature and pH stimuli.

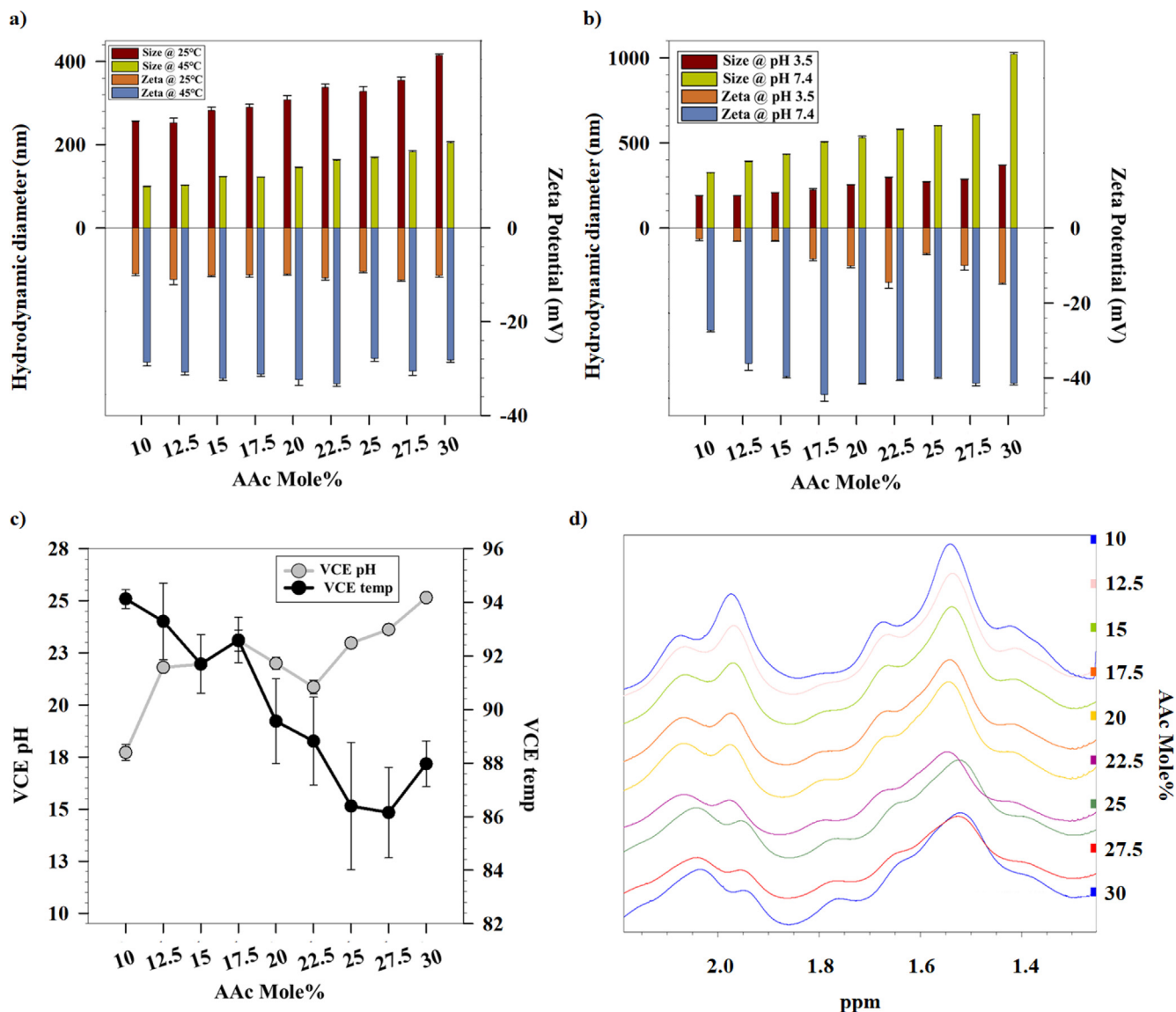| Sample	Temperature-based collapse 25–40 °C [%]	pH-based collapse synthesis pH – ph = 3.5 [%]
NGs_CS@AAc_10	93.4	6.8
NGs_CS@AAc_15	91.9	41.7
NGs_CS@AAc_25	88.6	51.3

Fig. 3. Hydrodynamic diameter and zeta potentials of the NGs, synthesised via the continuous-stirring method (NGs_CS) with different mole% of AAc, at a) 25 and 45 °C (at neutral pH), and b) pH = 3.5 and 7.4 (at 25 °C), showing the collapse of NGs at elevated temperature (above VPTT) and acidic pH conditions. c) Volumetric collapse efficiency of the NGs_CS with respect to pH and temperature, suggesting a decrease in temperature-based collapse and increase in pH-based collapse with increasing AAc mole%. The error bars represent the standard deviation calculated from the triplicate measurement of the particular sample. d) ^1H NMR spectra of NGs synthesized with increasing mole% of AAc, with the increase in peaks for pAAc with increasing AAc mole%, suggesting increased incorporation of pAAc in the NGs.

the protonation in acidic medium leads to greater amount of water extrusion from the NG pores due to breaking of hydrogen bonds resulting in greater collapse and, thus, higher VCE_{pH} when transitioning from pH = 7.4 to 3.5. An inverse trend in VCE_{temp} with increasing initial AAc content is observed. As the temperature dependent collapse is brought about by pNIPAm, the increased incorporation of AAc units in the NGs might suppress the temperature response to some extent thereby reducing the degree of collapse with increasing amounts of AAc units. In addition, the deprotonation of AAc might increase with temperature resulting in intermolecular repulsion that will additionally hinder collapse (opposing the collapse caused by pNIPAm). The effect of the presence of AAc units is evident for samples AAc_25, AAc_27.5 and AAc_30, where the VCE_{temp} tends to stabilize and even showing a slight increase in the case of AAc_30. To observe the higher content of pAAc in the NG matrix with increasing mole ratio of AAc reagent, ^1H NMR was performed. As the proton chemical shifts for pNIPAm and pAAc in the polymer backbone overlap in the region 1.4–

2.2 ppm, similar result was observed with these NGs. However, increased intensity could be seen at around 2.1 ppm and 1.75 ppm for the protons of pAAc (Fig. 3d). This increase could be due to the higher relative incorporation of AAc in the NG with increasing mole%.

Fig. 4a and b show the variation of hydrodynamic diameter of the NG with temperature and pH, respectively. The NGs show greater response with increasing initial AAc mole%, as is evident from the heating and cooling cycle curves for AAc_10, AAc_20 and AAc_30. This might be due to the lower content of NIPAm monomer units being incorporated in the NGs relative to the AAc. AAc_10 might have longer pNIPAm chains before being interrupted by pAAc chains (system has lower amount of AAc in the reaction mixture). For AAc_30, more AAc is present in the reaction mixture, facilitating pNIPAm co-polymerizing with pAAc, resulting in shorter pNIPAm chains (interpenetrated with pAAc). The range of collapse of the NGs depends on similar chain lengths formed by consecutive pNIPAm units before being interrupted by pAAc
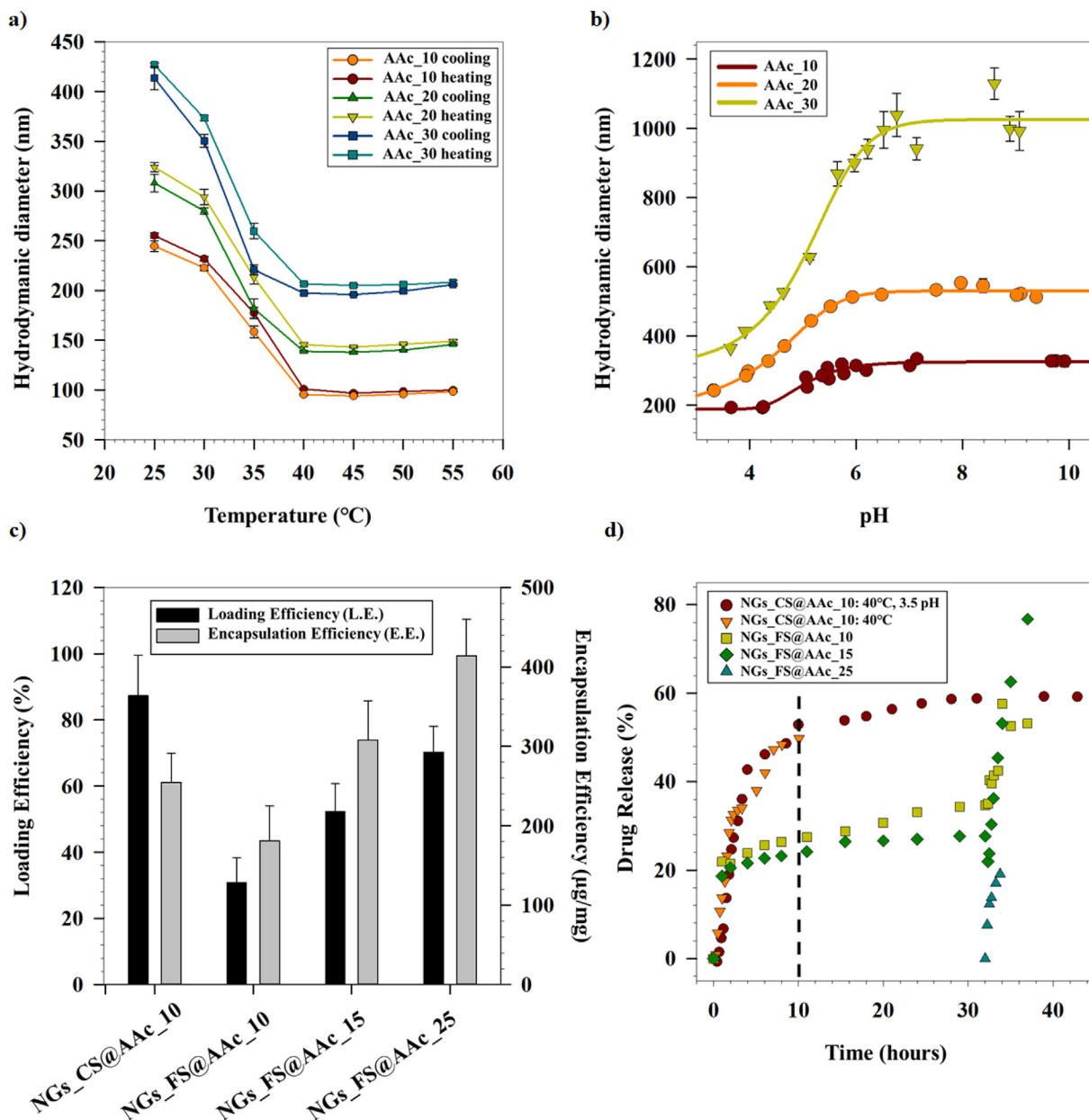
Fig. 4. Variation of the hydrodynamic diameter of AAc_10, AAc_20 and AAc_30 with respect to a) temperature and b) pH, showing decrease in size with increasing temperature and decreasing pH. c) Loading (L.E.) and encapsulation (E.E.) efficiencies of NGs_CS and NGs_FS, with the L.E. and E.E. for NGs_FS increasing with increasing AAc mole%. d) Release profiles of Cyt C from NGs_CS and NGs_FS at conditions of elevated temperature (>VPTT) and pH (acidic medium), mimicking cancerous microenvironment conditions. The error bars represent the standard deviation calculated from the triplicate measurement of the particular sample.

chains. Hence, pNIPAm chains with similar lengths will result in greater response (over a shorter range of temperature), whereas, NGs having different chain lengths of pNIPAm will have lower response (over a larger range of temperatures). Also, more responsive collapse of the NGs might be caused by the increased amounts of crosslinker (BIS) present in the samples with higher initial AAc mole % (Table 1). Larger number of crosslinker units will allow the NG to collapse to a larger extent thereby causing a greater hydrophilic to hydrophobic response. A similar sharp transition is observed with AAc_30, showing the sharpest variation in size when going from acidic to basic medium (Fig. 4b). Additionally, the increase in size for AAc_30 and AAc_20 occurs even at pH below 4, whereas AAc_10 only shows an increase after pH = 4.5. As can be seen from Fig. 3b, there is a slight increase in the zeta potential of the NGs with increasing basicity, which might indicate

more AAc units being present on the surface of the NGs. Therefore, it can be argued that the early response to change in pH is seen for AAc_30 and AAc_20 owing to more AAc units present on the surface. The hydrodynamic diameter for AAc_30 also seems to plateau off (size stops increasing with further increase in pH) at higher pH values than its counterparts (Fig. 4b). Deprotonation of AAc units might start from the NG's surface towards the core as the units present on the surface will be exposed first. Hence, as AAc_30 has the more AAc units present on the surface (along with more units in the overall NG matrix), size increases with increasing pH, as the change in stimuli is registered by them with the NG matrix swelling and imbibing water. Since NGs_CS and NGs_FS showed similar sizes and VCEs, drug loading and release studies, using Cyt C, were performed on these systems to further compare these two systems.

3.3. Drug loading and release

Fig. 4c shows the loading (L.E.) and encapsulation efficiencies (E.E.) of the NGs synthesized via the continuous-stirring and the flashing-stirring methods, with varying concentrations of AAc. The L.E. and E.E. for AAc_10 is higher for NGs_CS than the NGs_FS when using Cyt *C*. Although, it can be seen that the L. E. and E.E. increases with increasing amounts of AAc for NGs_FS, the L.E. remains lower than for NGs_CS system at AAc_10. The increase in the L.E. with increasing AAc content might be owing to the increase in NG particle size. Breathing-in technique was used to load Cyt *C*, where NGs with larger sizes have the capacity to imbibe more drug inside their matrix as they swell on coming in contact with drug solution. Previous research has shown that the heme ligand, located in the lysine-rich region of Cyt *C*, interacts with the negatively charged hydrogel units via Coulombic forces, resulting in polymer-protein complex formation [49,50]. Therefore, increasing number of carboxylic groups (as more AAc units are incorporated in the NG matrix) might lead to higher number of binding sites for Cyt *C* thereby increasing drug loading.

Owing to an increase in metabolism, cancer cells thrive in acidic medium. Hence, to mimic cancerous regions and elevated body temperatures, the release of Cyt *C* from the NGs was observed at conditions of 40 °C and acidic pH as shown in Fig. 4d. NGs_CS particles were continuously exposed to 40 °C, while NGs_FS particles were first subjected to pH = 3 for 30 h, followed by 40 °C and pH = 3. In the case of NGs_CS samples, the Cyt *C* release profiles at 40 °C and at 40 °C with pH = 3.5 coincided to a significant extent. It was seen that NGs_FS followed the release profile of NGs_CS for the initial part and almost plateaued out after a couple of hours. Drug release from NGs_CS was observed to be faster than NGs_FS with 50% of Cyt *C* being released in the first 10 h as opposed to 27% and 24% for NGs_FS@AAc_10 and NGs_FS@AAc_15 respectively. The high release could be attributed to a higher amount of Cyt *C* in NGs_CS (L.E. = 84.8 ± 12.2) resulting in a larger drive for diffusion because of higher concentration gradient. It is observed that temperature induces a greater collapse in the NGs as compared to pH, as shown in Table 4. Therefore, as the release for NGs_CS is induced by temperature and pH, there is a higher driving force (expelling the drug from the NG matrix) owing to greater NG collapse. On the contrary, no Cyt *C* release is seen for NGs_FS@AAc_25 when the system is exposed to just acidic pH condition, even though the system had higher L.E.. The release from this system occurs only after the temperature is raised above VPTT, to 40 °C. This fact, together with the similar release profiles for NGs_CS (40 °C and at 40 °C with pH = 3.5), further support the hypothesis that temperature has a greater impact on drug release than pH. Furthermore, the diffusion of Cyt *C* progresses in three probable zones. The first being transport of the drug from the NG matrix to the NG surface, second being transport of the drug from the NG's surface to the dialysis membrane, and the third, diffusion across the dialysis membrane into the sink. Owing to the larger size of the AAc_25 NGs, the drug needs to travel a greater distance (than AAc_10 and AAc_15) to reach the NG surface before it can diffuse out of the NG matrix. Thus, an excess push is needed to drive the drug out of the NG matrix, provided by the temperature stimuli.

Even though, the continuous and the flashing methods result in NGs having similar physico-chemical properties, the continuous method produces particles with a narrower size distribution with higher drug loading capacity. Furthermore, as NGs_CS had the highest VCE (91.9 ± 0.7) (Table 3), as well as L.E. (Fig. 4c), this system was selected for biocompatibility studies.

3.4. Whole blood responses

Cell viability of monocytes and granulocytes in human whole blood was maintained after exposure to the NGs, as compared to the PBS control and heat-killed cells (Fig. 5a). Complement activation was examined by measuring soluble TCC formation (Fig. 5b). NG exposure did not significantly increase the formation of TCC in human whole blood cells or activation of CR3 (Fig. S7). Therefore, it appears that the NGs neither significantly activate the complement system in human whole blood during the conditions examined, nor was production of the cytokines IL-1β, IL-6, IL-8 and TNF-α strongly affected compared to the baseline (PBS) values and positive controls. However, a minor, but not significant induction of IL-6 was noted with the highest NG dose, and minimal but statistical significant reduction in IL-8 and TNF-α was found for the intermediate NG doses. Previous research have reported similar data using other cell based models [34,35,51], however, whether the minimal decrease in IL-8 and TNF-α relative to the PBS control is biologically relevant can not be determined without vastly increasing number of donors to exclude potential statistical sampling errors. Minimal effects on complement activation, cytotoxicity and production of pro-inflammatory cytokines in human whole blood suggest that the NGs have good biocompatibility. On the other hand, there could be molecular processes induced by the NGs that are not accounted for by this model, such as production of other cytokines or increased cellular stress mechanisms, coagulation effects and tissue reactions during prolonged exposure *in vivo*. Thus, further investigations of these properties may be considered in order to fully develop these NGs as drug carriers.

4. Conclusion

Based on previous studies [10,4,24,25,38] new methods were developed to synthesize pNIPAm-pAAc-based nanogels (NGs), with varying degrees of physico-chemical properties. The physicochemical properties of the NGs are influenced by various parameters including reactant concentrations, temperature and reaction atmosphere. SDS has been shown to act as a stabilizing agent that affects particle size. The sizes of NGs reduced on increasing the concentration of SDS from 2.1 mM to 4.2 mM owing to the stabilization of the precursor particles during nucleation, as well as, a denser packing around the nucleation centres thereby preventing growth. In addition, the effect of reaction atmosphere (nitrogen) on the growth of the NGs was investigated using continuous and flashing techniques (with different stirring modes), namely – continuous-stirring (NGs_CS), flashing-stirring (NGs_FS) and flashing-impeller (NGs_FI). Although flashing methods produced uniform VCE$_{temp}$ on varying SDS, the NGs with the highest VCE$_{temp}$ were produced with the process having continuous supply of nitrogen to the reaction medium and highest SDS concentration (VCE$_{temp}$ = 92 ± 0%).

Furthermore, the pH responsiveness of NGs_CS was studied by varying AAc mole% during synthesis and the degree of pAAc incorporation in the NG matrix was confirmed by NMR. The size of NGs increased with increasing amounts of pAAc in the NG matrix and that also resulted in increased Cyt *C* loading efficiency (L.E.). L.E. was the highest for NGs_CS (L.E. = 87.4 ± 12.2%) compared to NGs_FS (L.E. = 30.8 ± 7.4%), for 10 mol% AAc. This study showed release of Cyt *C* with temp and pH, while controlling the particle size in nano-range. NGs_CS also showed biocompatibility, investigated by studying the activation of the complement system, and induced little or no release of pro-inflammatory cytokines/ chemokines in a human whole blood model. Further investigations, specifying the degree of incorporation of different monomer units in the NG matrix, along with studies on molecular processes
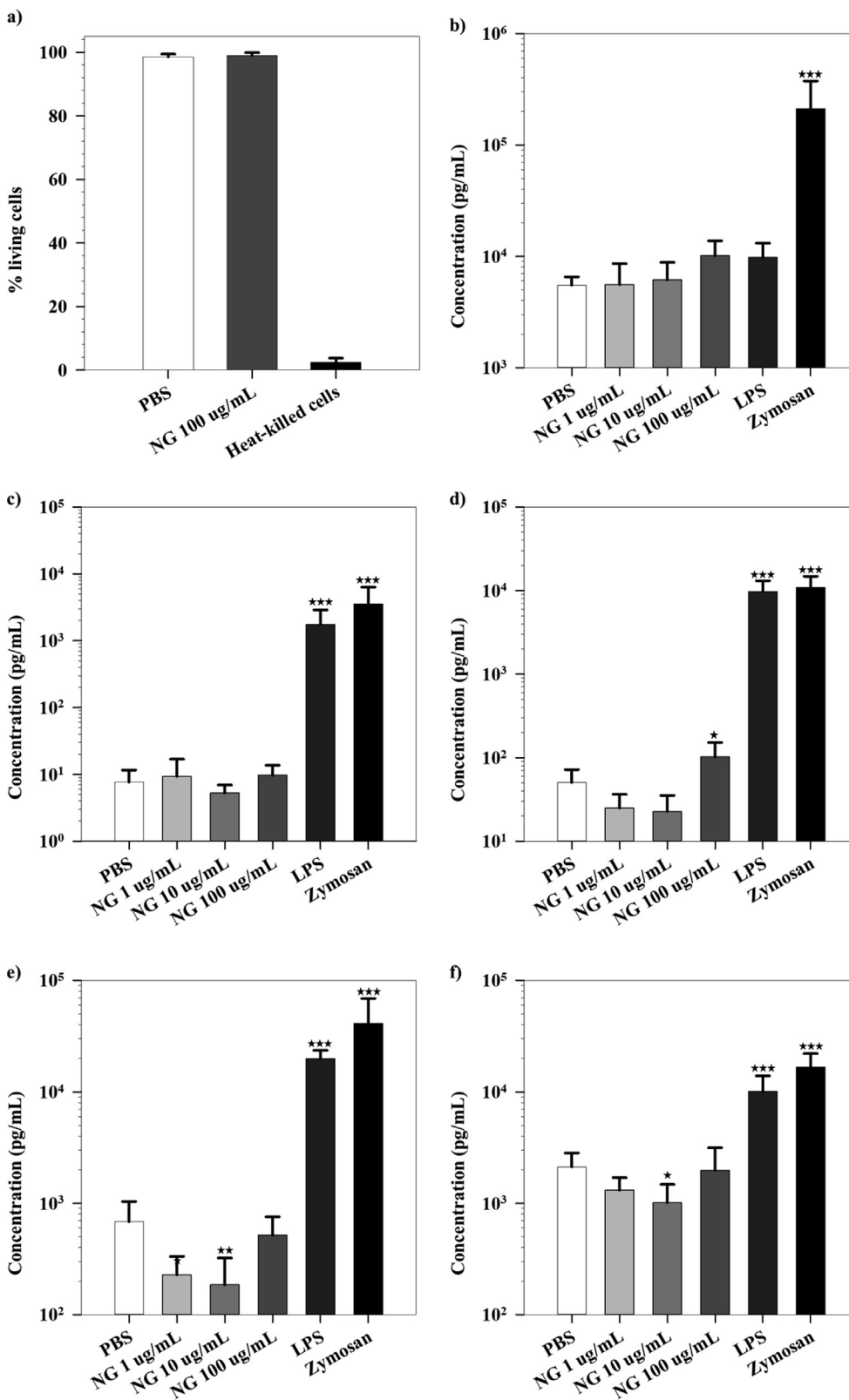
Fig. 5. a) Cell viability of monocytes and granulocytes was maintained after NG incubation in human whole blood. Loss of cell viability is accompanied by disruption of plasma membrane integrity and increased PI permeability and nuclear staining. Quantification of dead versus viable cells (PI intensity) was done by flow cytometry with gating for the respective cell types. b) There was no significant increase in TCC formation during incubation of NGs in blood, as determined by ELISA for soluble TCC in the plasma. c-f) Plasma levels of pro-inflammatory cytokines c) IL-1β, d) IL-6, e) TNF-α, and f) chemokine IL-8 were not significantly increased during NG incubation in blood, as determined by multiplex ELISA. For all subfigures: Error bars represent standard deviations. Statistical significance (*P<0.05, **P<0.01, ***P<0.001) compared to the PBS control found by 1way RM-ANOVA on log-transformed data (assuming log-normal distribution) with the Dunette post-test. N = 5 consecutive experiments.

induced in human blood, can help develop these NGs as drug carriers. Such drug carries can further incorporate metallic NPs, such as, gold, silver and iron-oxide, to impart optical and magnetic properties.

Ethics

The use of whole blood for these experiments was approved by the Regional Committee for Medical and Health Research Ethics in Central Norway (REC Central), The Norwegian Ministry of Education and Research, 2009/2245. Experiments were conducted according to their regulations and guidelines. Informed written consent was obtained from each voluntary donor prior to blood sampling.

Author's Contributions

All the NG synthesis, characterization and functionalization experiments have been performed at the Norwegian University of Science and Technology (NTNU), Norway.

CRediT authorship contribution statement

Anuvansh Sharma: Conceptualization, Methodology, Software, Validation, Investigation, Resources, Visualization, Writing – original draft, Writing – review & editing. **Karthik Raghunathan:** Conceptualization, Software, Validation, Investigation, Resources, Visualization, Writing – original draft, Writing – review & editing. **Helene Solhaug:** Conceptualization, Methodology, Validation, Investigation, Resources, Visualization, Writing – original draft, Writing – review & editing. **Jibin Antony:** Software, Validation, Investigation, Visualization. **Jørgen Stenvik:** Conceptualization, Methodology, Validation, Writing – original draft, Visualization, Supervision, Writing – review & editing. **Asbjørn Magne Nilsen:** Conceptualization, Methodology, Validation, Writing – original draft, Visualization, Supervision, Writing – review & editing. **Mari-Ann Einarsrud:** Validation, Visualization, Supervision, Writing – original draft. **Sulalit Bandyopadhyay:** Conceptualization, Methodology, Validation, Visualization, Supervision, Writing – original draft, Writing – review & editing.

Declaration of Competing Interest

The authors declare that they have no known competing financial interests or personal relationships that could have appeared to influence the work reported in this paper.

Appendix A. Supplementary material

Supplementary data associated with this article can be found, in the online version, at https://doi.org/10.1016/j.jcis.2021.07.139.

References

[1] L. Zha, B. Banik, F. Alexis, Soft Matter 7 (2011) 5908–5916.
[2] A.H. Bacelar, I.F. Cengiz, J. Silva-Correia, R.A. Sousa, J.M. Oliveira, R.L. Reisa, Handbook of intelligent scaffolds for tissue engineering and regenerative medicine 2 (2017) 327–361.
[3] N.K. Preman, R.R. Barki, A. Vijayan, S.G. Sanjeeva, R.P. Johnson, Eur. J. Pharm. Biopharm. (2020).
[4] R. Raju, S. Bandyopadhyay, A. Sharma, S.V. Gonzalez, P.H. Carlsen, O.R. Gautun, W.R. Glomm, Polymers 10 (2018) 309.
[5] W. Liwinska, I. Stanislawska, M. Lyp, Z. Stojek, E. Zabost, RSC Adv. 9 (2019) 13736–13748.
[6] A.S. Vikulina, S.T. Aleed, T. Paulraj, Y.A. Vladimirov, C. Duschl, R. Von Klitzing, D. Volodkin, PCCP 17 (2015) 12771–12777.
[7] Nothdurft, K., Muller, D. H., Murtz, S. D., Meyer, A. A., Guerzoni, L. P., Jans, A., Kuhne, A. J., De Laporte, L., Brands, T., Bardow, A., et al. Is the Microgel Collapse a Two-Step Process? Exploiting Cononsolvency to Probe the Collapse Dynamics of Poly-N-isopropylacrylamide (pNIPAM). The Journal of Physical Chemistry B 125 (2021) 1503–1512.
[8] T. Trongsatitkul, B.M. Budhlall, Colloids Surf., B 103 (2013) 244–252.
[9] I. Sanzari, E. Buratti, R. Huang, C.G. Tusan, F. Dinelli, N.D. Evans, T. Prodromakis, M. Bertoldo, Sci. Rep. 10 (2020) 1–14.
[10] S. Bandyopadhyay, M.K. Andersen, M.A.A. Alvi, A. Sharma, R. Raju, B.H. McDonagh, W.R. Glomm, Colloid Polym. Sci. 294 (2016) 1929–1942.
[11] Z. Meng, M.H. Smith, L.A. Lyon, Colloid Polym. Sci. 287 (2009) 277–285.
[12] G.R. Hendrickson, L.A. Lyon, Angew. Chem. Int. Ed. 49 (2010) 2193–2197.
[13] W. McPhee, K.C. Tam, R. Pelton, J. Colloid Interface Sci. 156 (1993) 24–30.
[14] B. Wedel, T. Brandel, J. Bookhold, T. Hellweg, ACS Omega 2 (2017) 84–90.
[15] W.H. Blackburn, L.A. Lyon, Colloid Polym. Sci. 286 (2008) 563–569.
[16] J.M. Knipe, N.A. Peppas, Regenerative Biomater. 1 (2014) 57–65.
[17] C. Decker, K. Moussa, Rapid Commun. 11 (1990) 159–167.
[18] C.W. Miller, C.E. Hoyle, S. Jönsson, C. Nason, T. Lee, W. Kuang, K. Viswanathan, N-vinylamides and Reduction of Oxygen Inhibition in Photopolymerization of Simple Acrylate Formulations, ACS Publications, 2003.
[19] V.V. Krongauz, C.P. Chawla, J. Dupre, Oxygen and Radical Photopolymerization in Films, ACS Publications, 2003.
[20] X. Xia, Z. Hu, Langmuir 20 (2004) 2094–2098.
[21] Y.K. Kim, E.-J. Kim, J.H. Lim, H.K. Cho, W.J. Hong, H.H. Jeon, B.G. Chung, Nanoscale Res. Lett. 14 (2019) 1–9.
[22] K. Kratz, T. Hellweg, W. Eimer, Colloids Surf., A 170 (2000) 137–149.
[23] V. Nigro, R. Angelini, B. Rosi, M. Bertoldo, E. Buratti, S. Casciardi, S. Sennato, B. Ruzicka, J. Colloid Interface Sci. 545 (2019) 210–219.
[24] S. Bandyopadhyay, A. Sharma, W.R. Glomm, Gels 3 (2017) 42.
[25] S. Bandyopadhyay, M.A.A. Alvi, A. Sharma, K. Zhu, A.-L. Kjøniksen, B. Nyström, W.R. Glomm, Colloid Polym. Sci. 295 (2017) 391–402.
[26] M.H. Smith, L.A. Lyon, Macromolecules 44 (2011) 8154–8160.
[27] A. Prasannan, H.-C. Tsai, Y.-S. Chen, G.-H. Hsiue, J. Mater. Chem. B 2 (2014) 1988–1997.
[28] D. Li, C.F. van Nostrum, E. Mastrobattista, T. Vermonden, W.E. Hennink, J. Controlled Release 259 (2017) 16–28.
[29] H. Zhang, Y. Zhai, J. Wang, G. Zhai, Mater. Sci. Eng.: C 60 (2016) 560–568.
[30] I. Neamtu, A.G. Rusu, A. Diaconu, L.E. Nita, A.P. Chiriac, Drug Deliv. 24 (2017) 539–557.
[31] Merkel, T. J., Jones, S. W., Herlihy, K. P., Kersey, F. R., Shields, A. R., Napier, M., Luft, J. C., Wu, H., Zamboni, W. C., Wang, A. Z., et al. Using mechanobiological mimicry of red blood cells to extend circulation times of hydrogel microparticles. Pro- ceedings of the National Academy of Sciences 2011, 108, 586–591.
[32] Halperin, J. A., Taratuska, A., Nicholson-Weller, A., et al. Terminal complement complex C5b-9 stimulates mitogenesis in 3T3 cells. The Journal of clinical investigation 1993, 91, 1974–1978.
[33] A. Fara, Z. Mitrev, R.A. Rosalia, B.M. Assas, Open Biol. 10 (2020) 200160.
[34] R.L. Bartlett, A. Panitch, Biomacromolecules 13 (2012) 2578–2584.
[35] Bridges AW, Singh N, Burns KL, Babensee JE, Andrew Lyon L, García AJ. Reduced acute inflammatory responses to microgel conformal coatings. Biomaterials.

2008 Dec;29(35):4605-15. https://doi.org/10.1016/j.biomaterials.2008.08.015. Epub 2008 Sep 19. PMID: 18804859; PMCID: PMC2585524.

[36] T.E. Mollnes, O.-L. Brekke, M. Fung, H. Fure, D. Christiansen, G. Bergseth, V. Videm, K.T. Lappegård, J. Kohl, J.D. Blood Lambris, J. Am. Soc. Hematol. 100 (2002) 1869–1877.

[37] M. Elsabahy, K.L. Wooley, Chem. Soc. Rev. 42 (2013) 5552–5576.

[38] S. Bandyopadhyay, A. Sharma, M.A.A. Alvi, R. Raju, W.R. Glomm, RSC Adv. 7 (2017) 53192–53202.

[39] K.S. Soppimath, L.-H. Liu, W.Y. Seow, S.-Q. Liu, R. Powell, P. Chan, Y.Y. Yang, Adv. Funct. Mater. 17 (2007) 355–362.

[40] Y. Chen, Y. Gao, L.P. da Silva, R.P. Pirraco, M. Ma, L. Yang, R.L. Reis, J. Chen, Polym. Chem. 9 (2018) 4063–4072.

[41] T.-Y. Liu, K.-H. Liu, D.-M. Liu, S.-Y. Chen, I.-W. Chen, Adv. Funct. Mater. 19 (2009) 616–623.

[42] H. Grüll, S. Langereis, J. Controlled Release 161 (2012) 317–327.

[43] Y. Kato, S. Ozawa, C. Miyamoto, Y. Maehata, A. Suzuki, T. Maeda, Y. Baba, Cancer Cell Int. 13 (2013) 1–8.

[44] E. Boedtkjer, S.F. Pedersen, Annual Rev. Physiol. 82 (2020) 103–126.

[45] L. Feng, Z. Dong, D. Tao, Y. Zhang, Z. Liu, National Sci. Rev. 5 (2018) 269–286.

[46] M.H. Smith, L.A. Lyon, Accounts Chem. Res. 45 (2012) 985–993.

[47] P. Pusey, J. Physique 48 (1987) 709–712.

[50] X. Gao, Y. Cao, X. Song, Z. Zhang, C. Xiao, C. He, X. Chen, J. Mater. Chem. B 1 (2013) 5578–5587.

[51] P.K. Jain, K.S. Lee, I.H. El-Sayed, M.A. El-Sayed, J. Phys. Chem. B 110 (2006) 7238–7248.

[52] V. Skobeleva, A. Zinchenko, V. Rogacheva, A. Zezin, Kabanov (2001) 43.

[53] M. Giulbudagian, G. Yealland, S. Hönzke, A. Edlich, B. Geisendörfer, B. Kleuser, S. Hedtrich, M. Calderón, Theranostics 8 (2018) 450.